Rock Mech Rock Eng (2011) 44:317–332
DOI 10.1007/s00603-010-0123-4

ORIGINAL PAPER

Numerical simulation of the rock fragmentation process induced by two drill bits subjected to static and dynamic (impact) loading

S. Y. Wang · S. W. Sloan · H. Y. Liu · C. A. Tang

Received: 22 June 2010 / Accepted: 19 October 2010 / Published online: 4 November 2010

Abstract Rock fragmentation processes induced by double drill bits subjected to static and dynamic loading are examined by a numerical method. Micro-heterogeneities of the rock are taken into account in this numerical model. For the static case, the simulated results reproduce the progressive process of brittle rock fragmentation during indentation. For the dynamic case, numerical simulations represent radial cracks, incipient chips, pulverized zones, and shell cracks. Comparing the static and dynamic cases, the dynamic loading can lead to rock fragmentation more efficiently. In addition, numerical results indicate that the dynamic pressure (P_{max}) plays an important role in the failure process of specimens with two indenters. Furthermore, the heterogeneity of the rock can also affect the failure modes of the rock when two indenters are used. Finally, the numerical results demonstrate the effect of the spacing between the indenters on the rock.

S. Y. Wang (✉) · S. W. Sloan
Centre for Geotechnical and Materials Modelling,
Civil, Surveying and Environmental Engineering,
The University of Newcastle, Callaghan,
NSW 2308, Australia
e-mail: Shanyong.Wang@newcastle.edu.au

S. W. Sloan
e-mail: Scott.Sloan@newcastle.edu.au

H. Y. Liu
School of Engineering, University of Tasmania,
Tasmania 7001, Australia
e-mail: Hong.Liu@utas.edu.au

C. A. Tang
School of Civil and Hydraulic Engineering,
Dalian University of Technology,
Dalian 116024, People's Republic of China
e-mail: catang@mechsoft.cn

Keywords Rock fragmentation · Numerical simulation · Indentation · Fracture process

1 Introduction

Rock fragmentation with a drill bit is an effective technique in mining engineering. Usually, the kinetic energy is transferred by means of a stress wave through the drill bit, until it reaches the end in contact with the medium to produce failure and fractures of rocks (Chiang 2004). Many experimental tests have been carried out in the past decades to investigate the mechanism of rock fragmentation (Wagner and Schumann 1971; Hustrulid and Fairhurst 1972; Lindqvist 1982; Cook et al. 1984; Pang and Goldsmith 1990; Lindqvist et al. 1994; Mishnaevsky Jr 1995; Kou 1995). These experiments have been essential for observing rock fragmentation phenomena and then to establish models to study failure mechanisms of rock due to mechanical tools. For example, researchers have performed indentation tests on different rocks subjected to indenters of various shapes and sizes, with the force-penetration behavior being recorded and the formation of craters and fractures being investigated (Lindqvist 1982; Cook et al. 1984; Pang and Goldsmith 1990). Based on experimental results, there are basically three systems of cracks according to their positions related to the indenter, i.e., side cracks, radial cracks, and median cracks (Kou 1995; Paul and Gangal 1969; Liu et al. 2008). Fully developed side cracks on each side of the indented area can connect with those induced by neighboring indenters to form chips. This forms the so-called conceptual model for fracture patterns induced by indenters (Kou 1995). In addition, Paul and Gangal (1969) reported that at the point of contact with the rock surface a bulb of very high hydrostatic pressure is

generated by the high bearing stresses. The general picture of fractures in rocks under indentation is summarized in Fig. 1. Many details can be added into this simple description (Lindqvist 1982; Kou 1995; Hood and Alehossein 2000; Detournay et al. 2008).

However, due to the anisotropy and heterogeneity of rock, the process of fracture initiation, propagation, and coalescence under mechanical indentation is rarely observed directly in standard laboratory tests. Moreover, it is also difficult for empirical and purely analytical models to study the complex problems of rock fragmentation with a drill bit due to their simplified assumptions. For example, the cavity expansion model was extended by Johnson (1985) for wedge or cone indentation in a Tresca material. Alehossein et al. (2000) used this model to predict the indentation of rock by blunt tools. However, this model is usually assumed that the material is homogeneous. Accordingly, the process of fracture propagation and interaction due to drill bit action in heterogeneous rock is difficult to understand with this model. Although fracture mechanics has been used to derive a simple analytical formula to evaluate the cutting or penetrating forces (Zhao et al. 1994), the heterogeneity of the rock is generally neglected in fracture mechanics models.

Numerical techniques based on the finite element method (FEM) have been developed to simulate the impact problem in rock drilling. Kumano (1980) proposed a model to study the rock response due to impact loads and simulated the impact of projectiles on granular and porous rock. In this model, it is assumed that all the kinetic energy of the projectile is used in crushing and plastic deformation, with the effect of wave propagation being neglected. Wang and Lehnhoff (1976) used a FEM model to simulate the chip formation due to penetration into the rock. Unfortunately, the dynamic interaction between the hammer and rock was not considered. Following this study, Han et al. (2005) proposed a numerical model to simulate multiple impacts, with the failure of the rock being based on a Mohr–Coulomb model with strain-softening behavior. In their study, the rock damping effect on the stress wave propagation was considered. As rocks are heterogeneous materials consisting of planes of weakness, voids, pores, and micro-cracks, these aspects should be considered when modeling rock fragmentation in drilling. In this regard, Liu (2004) developed and used R-T^{2D} (Tock–Tool interaction) (Liu 2004) to simulate successfully the rock fragmentation process induced by single and double indenters. The heterogeneity of rock was considered, and the progressive process of rock fragmentation during indentation was reproduced. However, the work was limited to the quasi-static state.

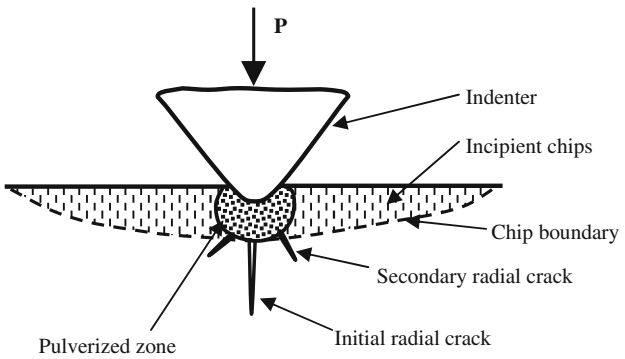

Fig. 1 Postulated fracture pattern under indenter loading. From Paul and Gangal (1969)

In this article, the numerical code RFPA^{2D} (Rock Failure Process Analysis, 2D) (Zhu and Tang 2006) is used to consider the heterogeneity of rock and simulate the evolution of dynamic fracture initiation and propagation due to impact loading from double indenters. The fracture characteristics of quasi-static and dynamic (impact) loading are compared using numerical simulations, and the influence of heterogeneity on fragmentation is studied. Furthermore, the effect of the dynamic pressure ($P_{\max}$) as well as the spacing between two indenters is investigated. It is noted that the effect of shape and the size of bits on rock fragmentation is not considered in the present study. In addition the indentation problem is simplified to a plain strain condition and the present model does not account for bit rotation addressed by Han et al. (2005).

2 Brief description of RFPA^{2D}

2.1 Assignment of material properties

In order to capture the heterogeneity of rock at the meso-level, the mechanical properties of each phase, including the elastic modulus, the strength and the Poisson's ratio, are all assumed to conform to the Weibull distribution as defined by the following probability density function:

$$f(u) = \frac{m}{u_0}\left(\frac{u}{u_0}\right)^{m-1} \exp\left[-\left(\frac{u}{u_0}\right)^{m}\right] \quad (1)$$

where u is a given mechanical property (such as the strength or elastic modulus), u_0 is a scale parameter and m is a shape parameter which defines the shape of the distribution function. In the present study, m defines the degree of material homogeneity and is thus referred to as the homogeneity index instead. This approach for assigning material properties has been shown to be an effective means of modeling the heterogeneity of rock and concrete (Tang 1997; Tang et al. 2000; Liu 2004; Zhu and Tang 2004, 2006).

2.2 Damage mechanics approach for meso-level modeling

In this model, the damage mechanics approach is employed to model the mechanical behavior of meso-scale elements. The stress–strain curve of each element is assumed to be linear elastic up to a damage threshold, followed by strain-softening. For each element, the material is assumed to be linear elastic, isotropic, and damage-free before loading (Liu 2004). After the initiation of damage, based on elastic damage mechanics, the elastic modulus of the element is assumed to degrade gradually as damage progresses, with the elastic modulus of the damaged material given by

$$E = (1 - D)E_0 \tag{2}$$

where D is the damage variable, and E and E_0 are the elastic moduli of the damaged and undamaged material, respectively. The damage variable D ranges from zero for the undamaged material to one, which represents the completely damaged state (Tang 1997).

2.2.1 Tensile failure

When the maximum tensile strain criterion is met, damage to the element occurs. Herein, this kind of damage is called tensile damage and D is given by

$$D = \begin{cases} 0 & \varepsilon < \varepsilon_{t0} \\ 1 - \frac{f_{tr}}{E_0 \varepsilon} & \varepsilon_{t0} \le \varepsilon < \varepsilon_{tu} \\ 1 & \varepsilon \ge \varepsilon_{tu} \end{cases} \tag{3}$$

where f_{tr} is the residual tensile strength, ε is the tensile strain, ε_{t0} is the tensile strain at the elastic limit (the so-called threshold strain), and ε_{tu} is the ultimate tensile strain corresponding to the completely damaged state of the material (Zhu and Tang 2004, 2006).

2.2.2 Shear failure

In the present mesomechanical model, the Mohr–Coulomb criterion is included as the second damage threshold to detect shear damage. This criterion is given by the following equation (Zhu and Tang 2004, 2006):

$$\sigma_1 - \frac{1 + \sin\phi}{1 - \sin\phi}\sigma_3 \ge f_{c0} \tag{4}$$

where σ_1 and σ_3 are the major and minor principal stresses, respectively, f_{c0} is the uniaxial compressive strength, and ϕ is the angle of internal friction. The damage variable D is given by

$$D = \begin{cases} 0 & \varepsilon < \varepsilon_{c0} \\ 1 - \frac{\sigma_{cr}}{E_0 \varepsilon} & \varepsilon \ge \varepsilon_{c0} \end{cases} \tag{5}$$

where σ_{cr} is the residual uniaxial compressive strength, ε_{c0} is the strain at the peak value of maximum principal stress (Zhu and Tang 2004).

It is believed that there must be a strong link between rock damage and the acoustic emission (AE) (Tang and Kaiser (1998). In RFPA^{2D}, the failure (or damage) of every element is assumed to be the source of an acoustic event because the failed element must release its elastic energy stored during the deformation. Therefore, by recording the number of damaged elements and the associated amount of energy release, RFPA^{2D} is capable of simulating AE activities, including the AE event rate, magnitude, and location. According to Tang and Kaiser (1998) the accumulative damage, D can be calculated by the following Eq. 6:

$$D = \frac{1}{N}\sum_{i=1}^{s} n_i \tag{6}$$

where s is the number of calculation steps, n_i is the damaged elements in the ith step and N is the total number of elements in the model. In addition, when the element fails, the energy released is calculated by Eq. 7 (Tang et al. 2007):

$$W_i = \frac{1}{2E}(\sigma_1^2 + \sigma_3^2 - 2v\sigma_1\sigma_3)V \tag{7}$$

where i is the element number, W_i is the released elastic strain energy, E is the elastic modulus, σ_1 and σ_3 is the major and minor principle stress, respectively, v is the Poisson ratio, and V is the element volume (Tang et al. 2007). AE activity indicates the extent of local damage in rock, which is directly associated with the evolution and propagation of fractures. By recording the counts of all failed elements and released energies when failure occurs, the AE phenomena associated with the progressive failure process can be simulated.

2.3 Strain-rate-dependent damage threshold

In order to consider the effects of strain rate on the failure mechanism of rock under dynamic loading, Zhao (2000) proposed that the Mohr–Coulomb criterion is applicable to dynamic loading condition if the cohesion is increased with increasing strain rate. This suggestion was based on a variety of experimental results for granite. The relation between the dynamic uniaxial compressive strength and the loading rate can be described with a semi-log formula as:

$$f_{cd} = A\log(\dot{f}_{cd}/\dot{f}_{c0}) + f_{c0} \tag{8}$$

where f_{cd} is the dynamic uniaxial compressive strength (MPa), $\dot{f}_{cd}$ is the dynamic loading rate (MPa/s), $\dot{f}_{c0}$ is the quasi-brittle loading rate (approximately 5×10^{-2} Mpa/s),

and f_{c0} is the uniaxial compressive strength at the quasi-static loading rate (Zhu and Tang 2006).

2.4 Finite element implementation

The rock specimen is assumed to be composed of many rectangular elements of the same size, which also act as four-noded isoparametric elements for finite element analysis. The equilibrium equations governing the linear dynamic response of a system of finite elements can be expressed in the following form (Zhu and Tang 2006).

$$\mathbf{M}\ddot{\mathbf{U}} + \mathbf{C}\dot{\mathbf{U}} + \mathbf{K}\mathbf{U} = \mathbf{R} \tag{9}$$

where **M**, **C** and **K** are the mass, damping, and stiffness matrices, **R** is the vector of externally applied loads, and **U**, $\dot{\mathbf{U}}$ and $\ddot{\mathbf{U}}$ are the displacement, velocity, and acceleration vectors, respectively. A lumped mass analysis is assumed, where the structure mass matrix is the sum of the individual element mass matrices concentrated at specified degrees of freedom (Zhu and Tang 2006). A direct step-by-step explicit integration procedure is adopted to solve the problem in which a body is subjected to impact loading. When the stain rate effect is considered and the maximum tensile strain criterion or Mohr–Coulomb criterion is met in the elements, the stresses are re-analyzed iteratively using the current boundary conditions in order to reflect the stress redistribution at the current time step. The program does not proceed to the next time step until no new damaged elements are found during this iterative process (Zhu and Tang 2006).

Note that the constitutive law described above has been applied and proved successful for modeling the failure of rock specimens under various static and dynamic stress conditions (Tang 1997; Tang et al. 2000; Liu 2004; Zhu and Tang 2004, 2006; Wang et al. 2006, 2010).

3 Model setup

In the following series of numerical simulations, the indentation problem is simplified to a plain strain condition as shown in Fig. 2a, b. Figure 2a is for the quasi-static case, and Fig. 2b is for the dynamic case. For the quasi-static case, a constant velocity (0.005 mm/step) is applied to the indenters, and a lateral confining pressure of 0 or 5 MPa acts on the sides of the rock specimen. For the dynamic case, three kinds of compressive stress waves are applied, as shown in Fig. 3. Furthermore, different values of the homogeneous index (m) of the rock and different spacings between the two indenters are considered.

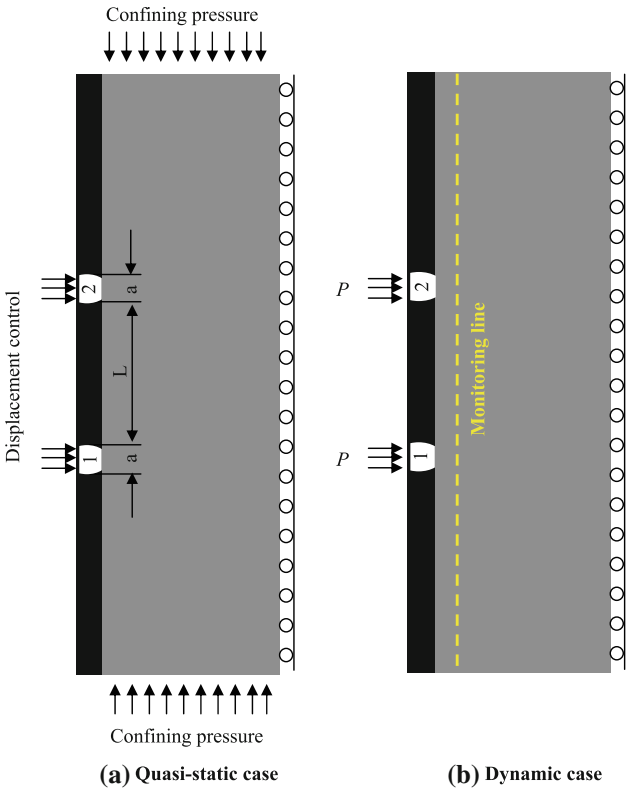

Fig. 2 Mechanical model of numerical simulation

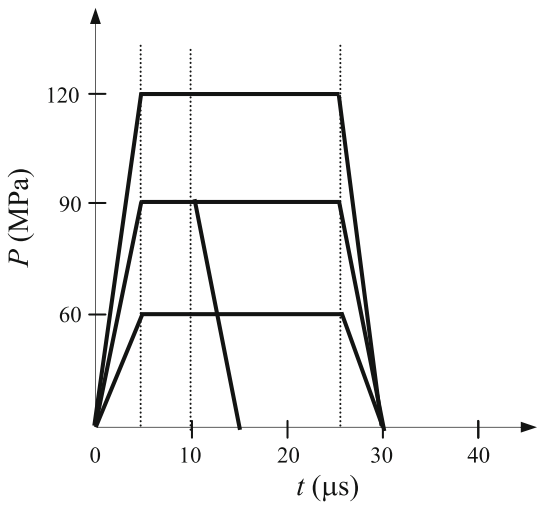

Fig. 3 Dynamic impact compressive stress waves applied on the top surfaces of two indenters

In these simulations, the mesh size of each model is 100 × 300 with 30,000 elements used to simulate a 1 m × 3 m rock mass. All the elements in the indenter have the same mechanical parameters. As for the rock, because of its heterogeneity, each element contains an unequal number of defects, and therefore, possesses different mechanical properties. This follows from the use of the Weibull distribution described in Eq. 4. The basic

parameters for the static and dynamic models are listed in Tables 1 and 2, respectively. The strength and elastic modulus of the indenters in the current models have a sufficiently high value so that the indenters will not fail during failure of the rock (see Table 3). More descriptions of numerical simulations for rocks under static and dynamic loading can be found in previous publications (Zhu and Tang 2006).

4 Numerical results for the rock fragmentation process (quasi-static) induced by double indenters

4.1 Formation of the crack system

Figure 4a, b shows, respectively, numerical simulations of the rock fragmentation process due to two indenters under quasi-static loading with lateral confining pressures of 0 and 5 MPa. When the indenter acts on the rock, a fan-shaped field of high stress is created immediately beneath the two indenters, as shown in stage A in Fig. 4a. With increasing load, one or more flaws initiate and nucleate to form an initial radial crack around the corners of indenter (see Fig. 4a, stage B) (Liu et al. 2002; Liu 2004). Due to the heterogeneity of rock, the paths for these initial radial cracks are not identical, with the crack from indenter 1 growing faster than the crack from indenter 2. Simultaneously, some incipient chips develop between the two indenters due to the interacting stress fields which enhance the initiation of fractures (Liu et al. 2002). These chips are caused by the tensile cracks emanating from the lateral face (see Fig. 4a, stage B). With further indenter displacement, the initial radial cracks continue to develop (Fig. 4a, stage C) and numerous small secondary radial cracks start to initiate and develop. Additional incipient chips also occur, especially around one side of indenter 2, and with increasing stress all the cracks propagate forwards (Fig. 4a, stage D). Due to high stress, the elements beneath the indenters fail and pulverized zone starts to form (Fig. 4a, state E).

Table 1 Material properties of specimens for quasi-static models

Parameter	Value
Homogeneity index (m) of the matrix	3
Mean compressive strength (σ_0)	300 MPa
Mean elastic modulus (E_0)	30,000 MPa
Ratio of compressive and tensile strength	10
Friction angle (φ)	30
Confining pressure (MPa)	0.5
Poisson ratio (μ)	0.25

Table 2 Material properties of specimens for dynamic models

Parameter	Value
Homogeneity index (m)	2, 6, 9
Mean elastic modulus (E_0)	30,000 MPa
Mean compressive strength (σ_0)	300 MPa
Ratio of compressive and tensile strength	10
Poisson ratio (μ)	0.25
Time step (μs)	0.2
One-dimensional wave velocity c (m/s)	3,500
L/a (L is space between two indenters, a is the width of indenter)	2, 4.67, 7.33

Table 3 Material parameters for indenters

Parameter	Value
Mean elastic modulus (E_0)	200 GPa
Mean compressive strength (σ_0)	1,000 MPa
Poisson ratio (μ)	0.25
Homogeneity index (m)	20

When the lateral compressive pressure is 5 MPa, the incipient chips occur on both sides of the indenters because of the high confining pressure. Comparing with zero confining stress case (Fig. 4a, stage A), more chips are concentrated in the zone between the two indenters due to the interaction of the higher stress fields (Fig. 4b, stage A). Under increasing loading, the rock beneath indenter 1 does not fail, even though it is highly stressed, due to the higher confining pressure. Initial radial cracks initiate first on both corners of the indenter, with the initial radial crack closer to indenter 2 developing faster (Stages B–E). For indenter 2, both initial and secondary cracks initiate and propagate to form cone cracks (Stages B–E) (Liu et al. 2002) which are unsymmetric because of the rock heterogeneity. As the penetration displacement increases, the incipient chips on both sides of the indenter propagate to form almost symmetrical shapes (Fig. 4b, stage D). Finally, more and more elements beneath the indenters fail and a pulverized zone is formed (Fig. 4b, stage E).

4.2 Force–penetration curve

Figures 5 and 7 show, respectively, the simulated force–penetration curves and associated AE counts during the rock fragmentation process induced by two indenters with lateral confining stresses of 0 and 5 MPa. Figures 6 and 8 present, respectively, the associated elastic energy release (ENR) and accumulated ENR versus displacement responses during rock fragmentation. The letters A–E

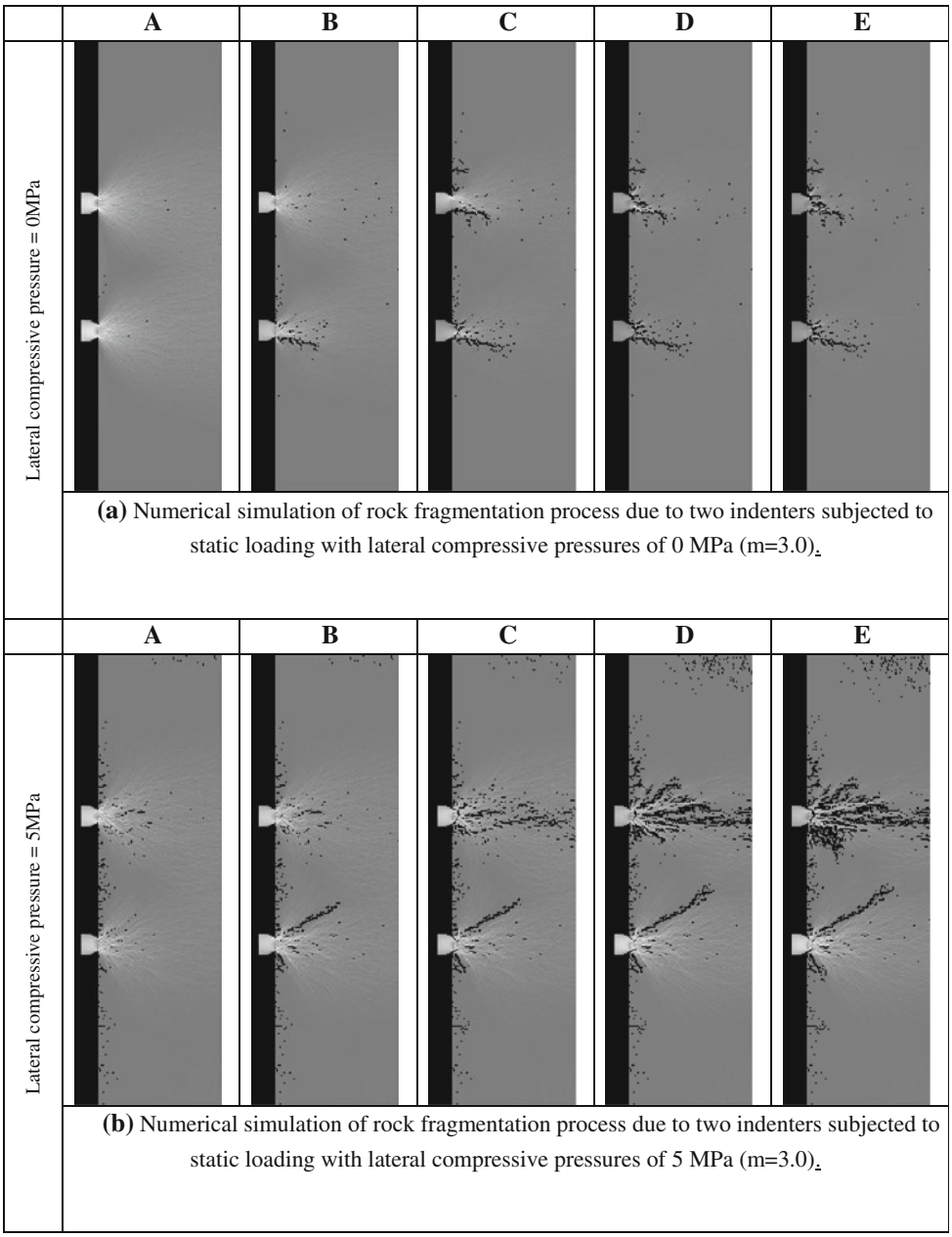

Fig. 4 Comparison of the numerical simulated rock fragmentation process due to the effect of the confining pressure

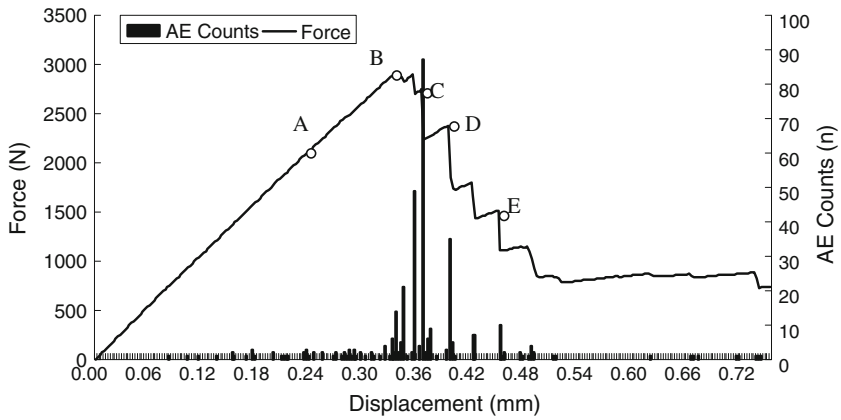

Fig. 5 Force–penetration curve during rock fragmentation by two indenters subjected to quasi-static loading with a lateral compressive stress of 0 MPa (strain control) ($m = 3.0$)

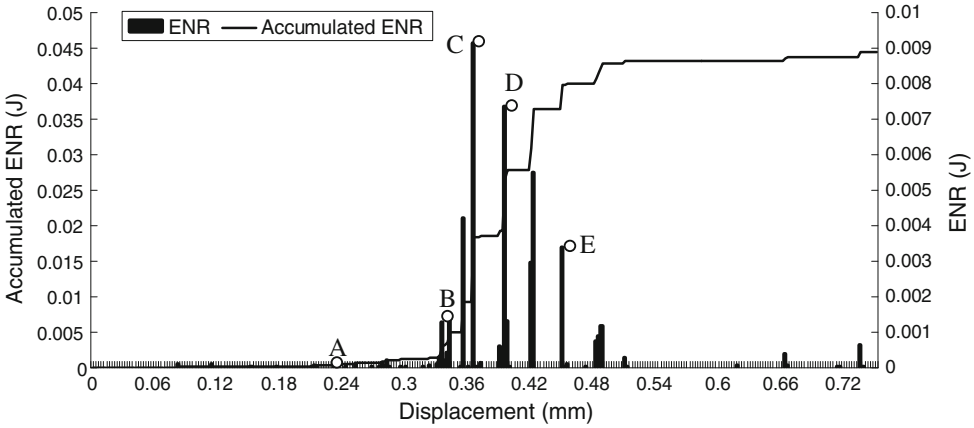

Fig. 6 Elastic energy release (ENR), accumulated ENR, and displacement curve during rock fragmentation by two indenters subjected to quasi-static loading with a lateral compressive stress of 0 MPa (strain control) ($m = 3.0$)

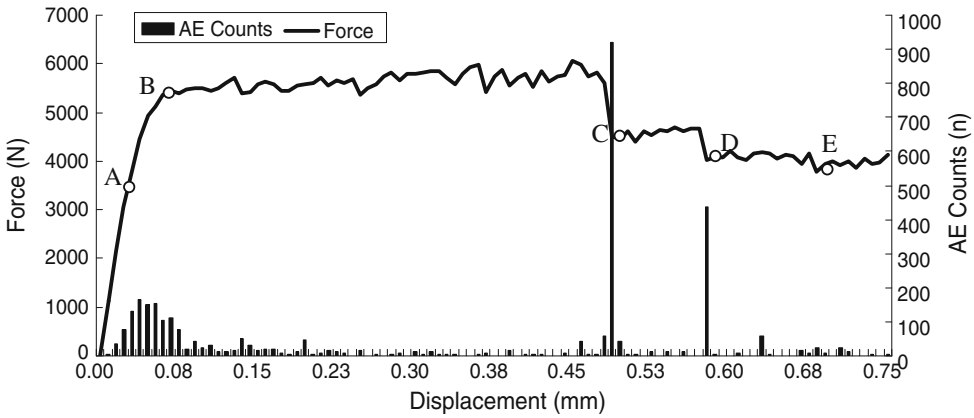

Fig. 7 Force–penetration curve during rock fragmentation by two indenters subjected to quasi-static loading with lateral compressive stress of 5 MPa (strain control) ($m = 3.0$)

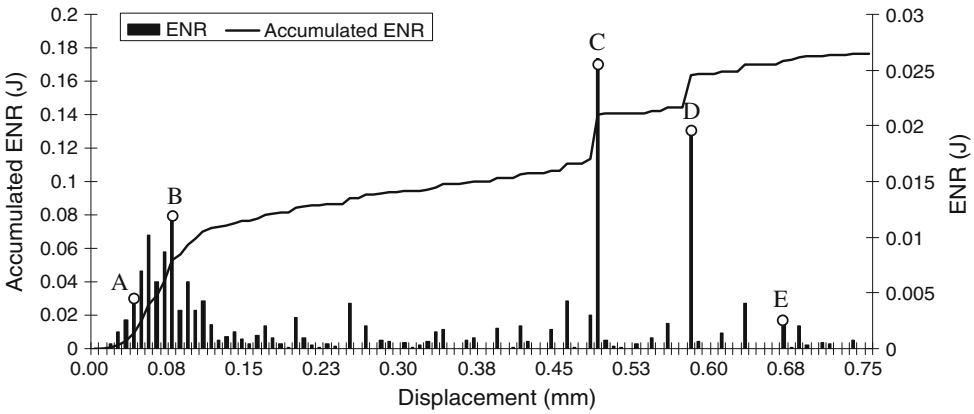

Fig. 8 Elastic energy release (ENR), accumulated ENR, and displacement curve during rock fragmentation by two indenters subjected to quasi-static loading with a lateral compressive stress of 5 MPa (strain control) ($m = 3.0$)

correspond to the same stages marked in Figs. 4a, b. From Figs. 5 and 7, it is shown that the force-penetration curve has almost a linear shape before point (A), due to the fact that little damage occurs up to this point. With increasing loading, the force–penetration curve attains its first peak value at point B, where the initial radial cracks occur. In order to examine the effect of confining pressure, we note that the peak value for point B is 2900 N in Fig. 5 and 5400 N in Fig. 7. The obvious force drops at points C, D, and E in Figs. 5 and 7 is caused by the rapid development of cracking in this stage of loading. The corresponding AE energy released is shown in Figs. 6 and 8. Due to the lateral compressive pressure, the load–displacement curve from point B has many small corrugations. These are indications

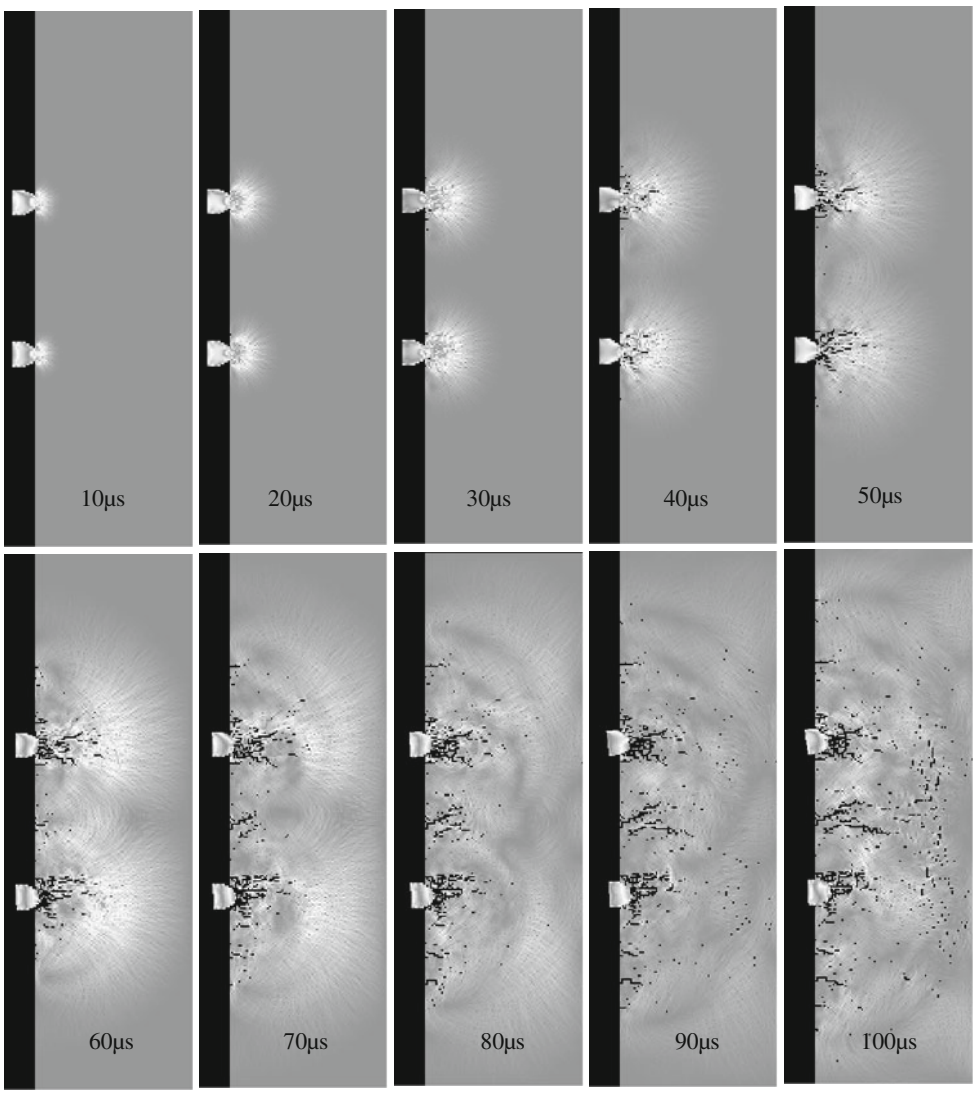

Fig. 9 Numerical simulation of fracture process of specimen due to impact loading with an amplitude of 90 MPa ($m = 3.0$)

of the propagation of fractures as well as the formation of small chips (Liu et al. 2002).

5 Numerical results for the rock fragmentation process due to dynamic (impact) loading

5.1 Dynamic fracture process due to impact loading

Figure 9 shows the numerical simulation of the fracture process of a specimen under impact loading. The maximum stress (P_{max}) of the compressive stress wave is 90 MPa. The duration of the incident compressive stresses is fixed to be 15 μs and the homogeneity index of the rock specimen is 3. During the first stage of loading ($t \leq 50$ μs), the stress fields induced by the double indenters are similar to those induced by quasi-static loading (Fig. 4a). The rock immediately below the indenters is highly stressed with a few radial cracks being initiated. However, with the two impact points causing compressive stress waves to propagate, a few circular-front cracks centered on the impact point are seen to emerge 60 μs after impact (when the two compressive waves meet and interfere). Some obvious tensile cracks are formed along the lateral face between the two indenters, and these propagate quickly ($60 \leq t \leq 90$ μs). Simultaneously, there are also some tensile cracks on the other side of the two indenters, which form the incipient chips. These cracks grow more slowly than those between the two indenters.

In addition, a few circular-front cracks are seen to emerge 100 μs after impact. These cracks, known as "shell cracks", are due to the condition of unconfined compression and are similar to the splitting observed in uniaxial compression tests performed on concrete or rock (Grange et al. 2008). It is interesting to note that radial cracking stops 70 μs after impact, with only tensile cracking on the lateral face and the shell cracking occurring. This is

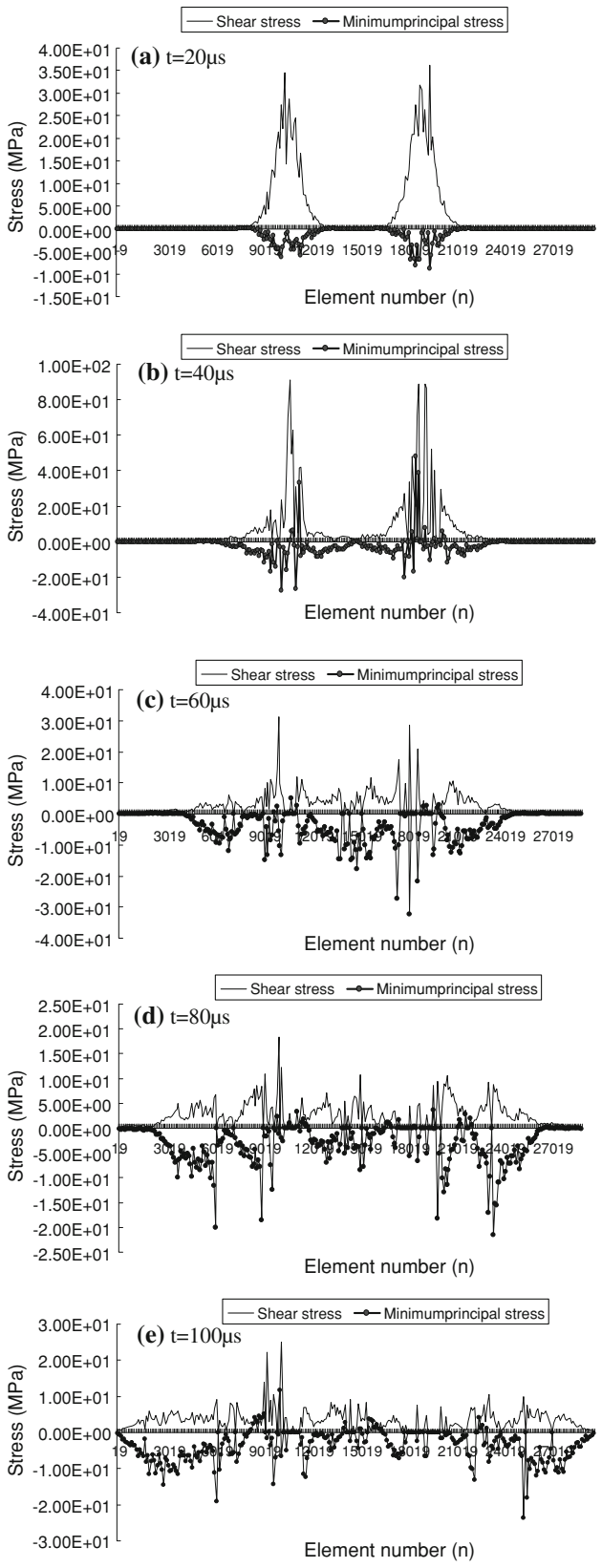

Fig. 10 Numerically simulated stress distributions along the monitoring line with time equal 20, 40, 60, 80, and 100 μs

different to the quasi-static case, where the radial cracks continue to propagate throughout the whole failure process.

Figure 10 shows the numerically predicted maximum shear stress and minimum principal stress distributions along the monitoring line (Fig. 2b) when t is 20, 40, 60, 80, and 100 μs. In Fig. 10a, when t is less than 20 μs, the stress fields do not interfere since the compressive stress waves from two indenters have not yet met. However, when t is 60 μs, the shear stress fields between the two indenters interact (Fig. 10c) which causes tensile cracks on each side of the indenters to initiate and propagate from the lateral face. The stress distribution along the monitoring line expands, also indicating the development of tensile cracks from each side of the two indenters when t reaches 80 μs (Fig. 10d). Finally, the shear stress and minimum principal stress distributions along the monitoring line are presented in Fig. 10e, when the shell cracks form and develop.

5.2 Effect of the amplitude of the incident pressure

Figure 11 presents the numerically simulated effects of three kinds of impact pressure on the two indenters. The maximum values (P_{max}) of the three kinds of compressive stress waves are 60, 90, and 120 MPa, respectively, as shown in Fig. 3. The durations of the incident compressive stresses are fixed to be 30 μs, and the homogeneity index of the rock specimen is set to 3. From Fig. 11, when t is 10 μs, there are no differences for the rock specimens subjected to different impact loadings. The rock under the indenters is highly stressed, but no micro-fractures are observed. When t is 20 μs, for the smaller P_{max} of 60 MPa, only some micro-fractures form beneath the two indenters with very few occurring beside them. For the middle P_{max} of 90 MPa, more micro-fractures occur both beneath and beside the two indenters. However, for the highest P_{max} of 120 MPa, although several bigger fractures form beneath the two indenters, fewer fractures occur beside the indenters than in the case of $P_{max} = 90$ MPa. When t is 30, 40, and 50 μs, more radial cracks are formed between the indenters, as well as tensile cracks along the lateral face. Comparing the three different impact compressive waves, it is only for $P_{max} = 90$ MPa that the cracks are great in number and develop fast, which leads to the most effective fragmentation. This indicates that the highest P_{max} does not give the greatest fragmentation of the rock.

It was well known that acoustic emission (AE) can be due to micro-fractures occurring when rock is subjected to dynamic loading. Accordingly, the degree of damage can be expressed by the AE number and the AE energy released (Tang 1997). Figure 12 shows numerical AE counts versus time due to impact loading for P_{max} of 60, 90

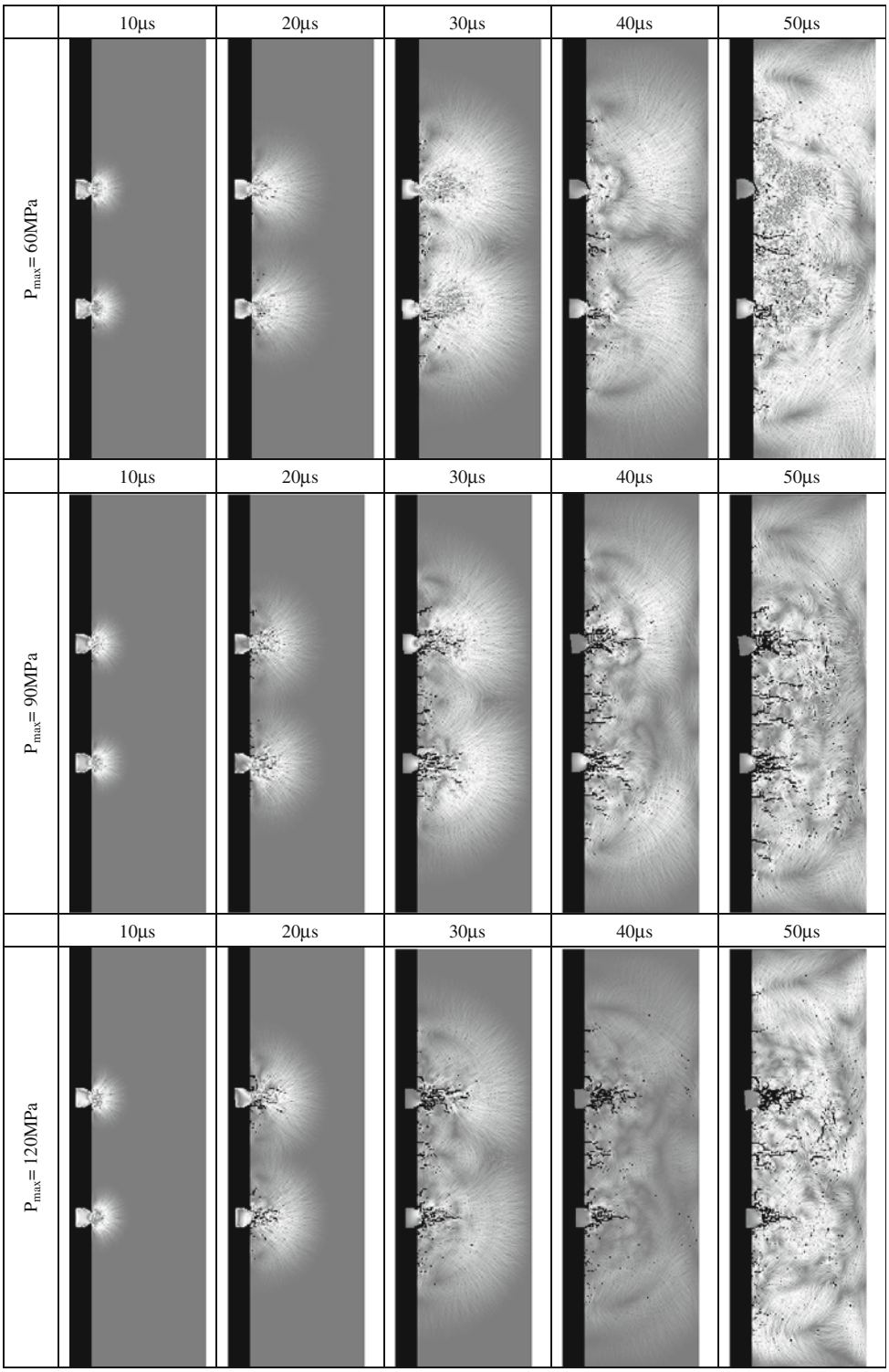

Fig. 11 Numerical simulation of the effect of three kinds of compressive stress waves on the failure process of specimens due to two indenters ($m = 3$)

and 120 MPa. Figure 13 presents the numerical simulation of released AE energy versus time. From Fig. 12, it is shown that the AE counts are greatest for the case of $P_{\max} = 120$ MPa when $t \leq 20$ μs. However, in the subsequent stage ($20 \leq t \leq 50$ μs), the AE counts are greatest for the case of a $P_{\max}$ of 90 MPa. When $t \geq 50$ μs, the AE counts are greatest for the case of a $P_{\max}$ of 60 MPa. From Fig. 13, the AE energy released for the case of $P_{\max} = 60$ MPa is the smallest during the whole process, while in the early stages ($t \leq 20$ μs) the released AE energy is largest for the case of $P_{\max} = 120$ MPa. However, during the period 20 μs $\leq t \leq$ 35 μs the released AE

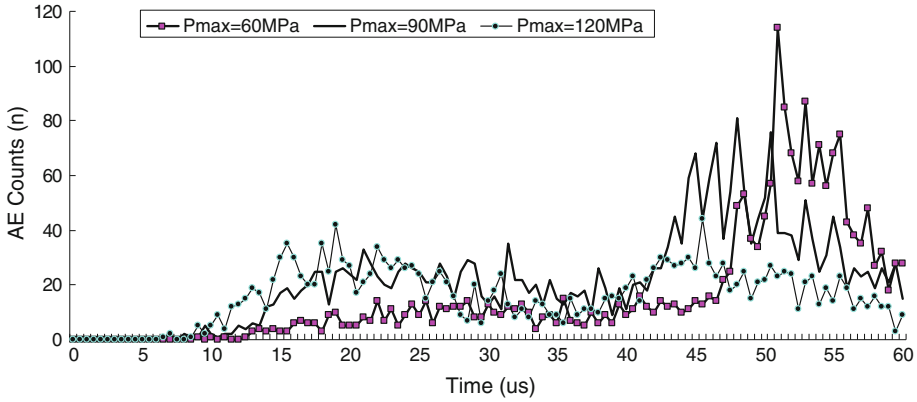

Fig. 12 Numerical simulation of AE counts versus time due to impact loading with P_{max} of 60, 90, and 120 MPa ($m = 3.0$)

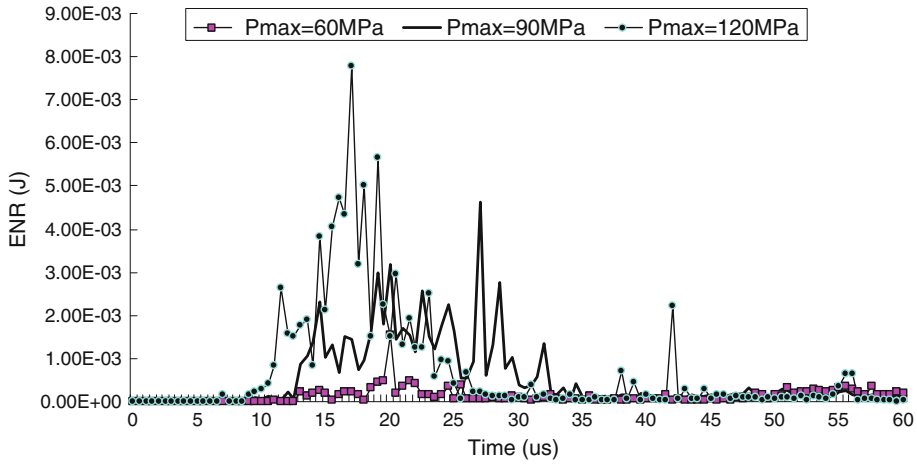

Fig. 13 Numerical simulation of AE energy versus time due to impact loading with P_{max} of 60, 90, and 120 MPa ($m = 3.0$)

energy is the largest for $P_{max} = 90$ MPa. These results indicate that an appropriate applied P_{max} for the compressive stress waves is very important for the efficient fragmentation of rock. Of course the efficiency of rock fragmentation also depends on other factors, such as the heterogeneity and the spacing between the indenters, and this is investigated in the following sections.

5.3 Influence of rock heterogeneity

All the analyses described so far assumed that the homogeneity index (m) was 3. Additional analyses were also performed for $m = 2$, 6, and 9 to examine the influence of rock inhomogeneity on the fracture patterns associated with two indenters under impact loading. These three cases correspond to heterogeneous, relatively homogeneous and very homogeneous rock, respectively. A maximum amplitude of $P_{max} = 90$ MPa in the compressive stress wave was applied for the various cases, with the duration of the incident compressive stresses set to 30 μs. Figure 14 shows the simulated effect of the homogeneity index (m) on the overall failure process. Shortly after loading when $t = 10$ μs, some fractures occur beneath the indenters for the heterogeneous case ($m = 2$), while there are no fractures for the other cases ($m = 6$, 9). Afterwards, when $t = 20$ μs, radial cracks form for the heterogeneous case, while only tensile cracks occur beside the indenters for the other cases. During later stages of dynamic loading, when 30 μs $\leq t \leq$ 50 μs, radial cracks are developed only for the heterogeneous case. In the other cases, only tensile cracks develop beside the two indenters.

Figures 15 and 16 show, respectively, plots of the numerical AE counts and AE energy release versus time for the homogeneity indices of $m = 2$, 6, and 9. In the initial stage of loading ($t \leq 40$ μs), both the AE counts and energy release are greater for the heterogeneous case. However, in the next stage ($t \geq 50$ μs), this situation is reversed. This is because the heterogeneous rock contains more structural particles, voids and fractures, either pre-existing or induced by stresses, which absorb more energy from the applied compressive stress waves. As a result, the compressive stress wave attenuation is more evident in heterogeneous rock.

5.4 Effect of the spacing of adjacent indenters on the fragmentation of rocks

The efficiency of rock drilling is strongly dependent on the separation between adjacent indenters, and is very

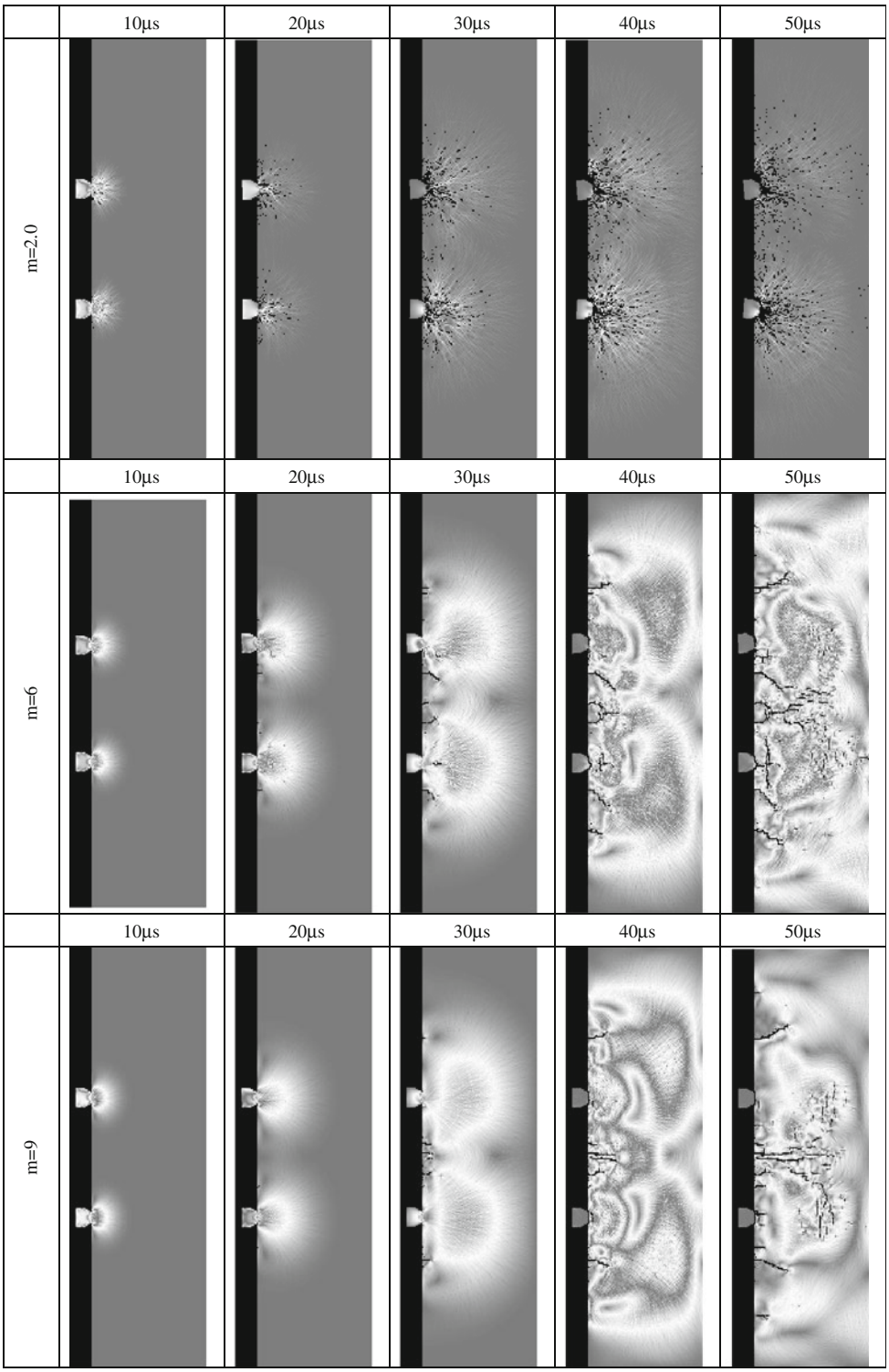

Fig. 14 Numerical simulation of the effect of the homogeneity index (m) on the failure process of specimens due to two indenters subjected to impact loading

important in the design and operation of machines (Liu et al. 2002). In this section, a normalized spacing (L/a) is used to study this effect, where L is the distance between the edge of adjacent indenters and a is the diameter of each indenter (see Fig. 2). Figure 17 shows the simulated results for rock fragmentation induced by double indenters with L/a values of 2, 4.67, and 7.66. For the smallest spacing, the interaction of the stress fields is incomplete (Liu et al. 2002), and the propagation of the compressive stress waves for double indenters is similar to that for a single indenter. When L/a is 4.67 the indenters act independently in the zones adjacent to the indenters and interact with each other

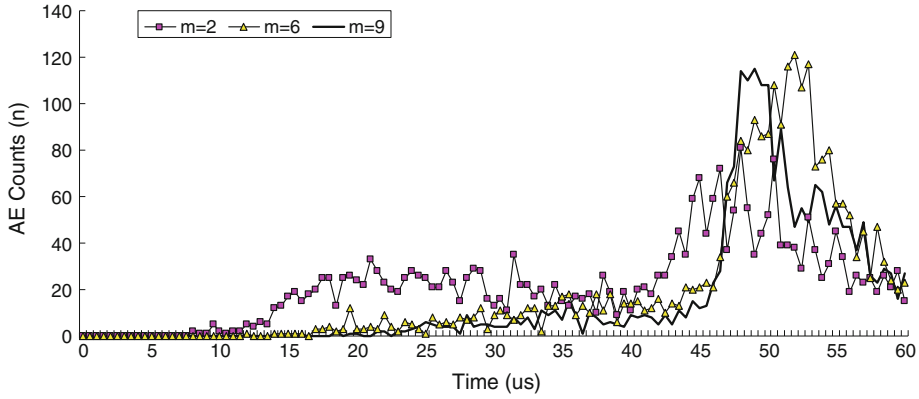

Fig. 15 Numerical simulation of AE counts versus time due to impact loading with maximum pressures of 90 MPa and m of 2.0, 6.0, and 9.0

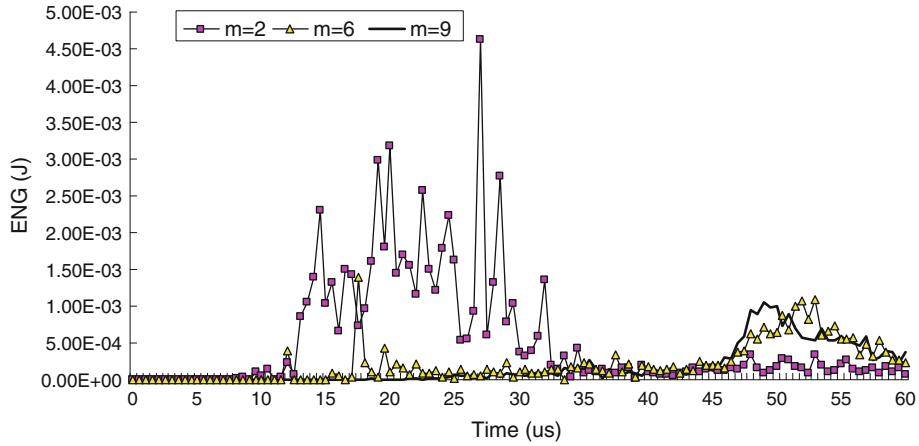

Fig. 16 Numerical simulation of AE energy versus time due to impact loading with maximum pressures of 90 MPa and m of 2.0, 6.0, and 9.0

in the zone between the indenters. Compared to the smaller spacing, this larger spacing is more effective at fragmenting the rock in terms of the energy cost of each indenter. For the largest spacing of $L/a = 7.66$, there are fewer tensile cracks between the two indenters. This suggests that a smaller spacing is needed to form larger chips and minimize the total energy consumed.

Figures 18 and 19 show, respectively, numerical simulations of the AE counts and released energy versus time due to impact loading with normalized spacings of $L/a = 2$, 4.67 and 7.66, respectively. It is shown that both the AE counts and released energy for L/a of 2 and 4.67 are greater than those of L/a of 7.66, and the higher AE counts and energy for the normalized spacing of 4.67 is higher than those of L/a of 2. This shows that the above analysis is reasonable.

6 Conclusions

In this study, the RFPA^{2D} code was applied to simulate quasi-static and dynamic (impact) rock fragmentation due to two indenters. Although reality is often much more complex than the numerical models used, the study provides interesting indications for improving the performance of rock fragmentation in indentation. From the numerical simulations, the following conclusions are derived.

(1) For the quasi-static case, numerical simulations reproduce the radial cracks, incipient chips and pulverized zone during the fragmentation of rock. The incipient chips are actually composed of many small tensile cracks from the lateral face. When the lateral confining pressure is zero, the region of radial failure extends completely beneath the punch. When a lateral confining pressure is applied, there is an increase in the indentation strength.

(2) For the dynamic case, numerical simulations also reproduce the radial cracks, incipient chips, pulverized zone and shell cracks. Comparing the static and dynamic cases, dynamic loading can lead to more efficient rock fragmentation. In addition, the numerical results indicate that it is not necessarily the highest amplitude of compressive stress wave that leads to the best fragmentation. To maximize the efficiency of the indenters, it is necessary to use an appropriate stress wave amplitude.

(3) For homogeneous rock, the dynamic numerical results show a smooth tensile crack from the left lateral face. In heterogeneous rock, the fractures

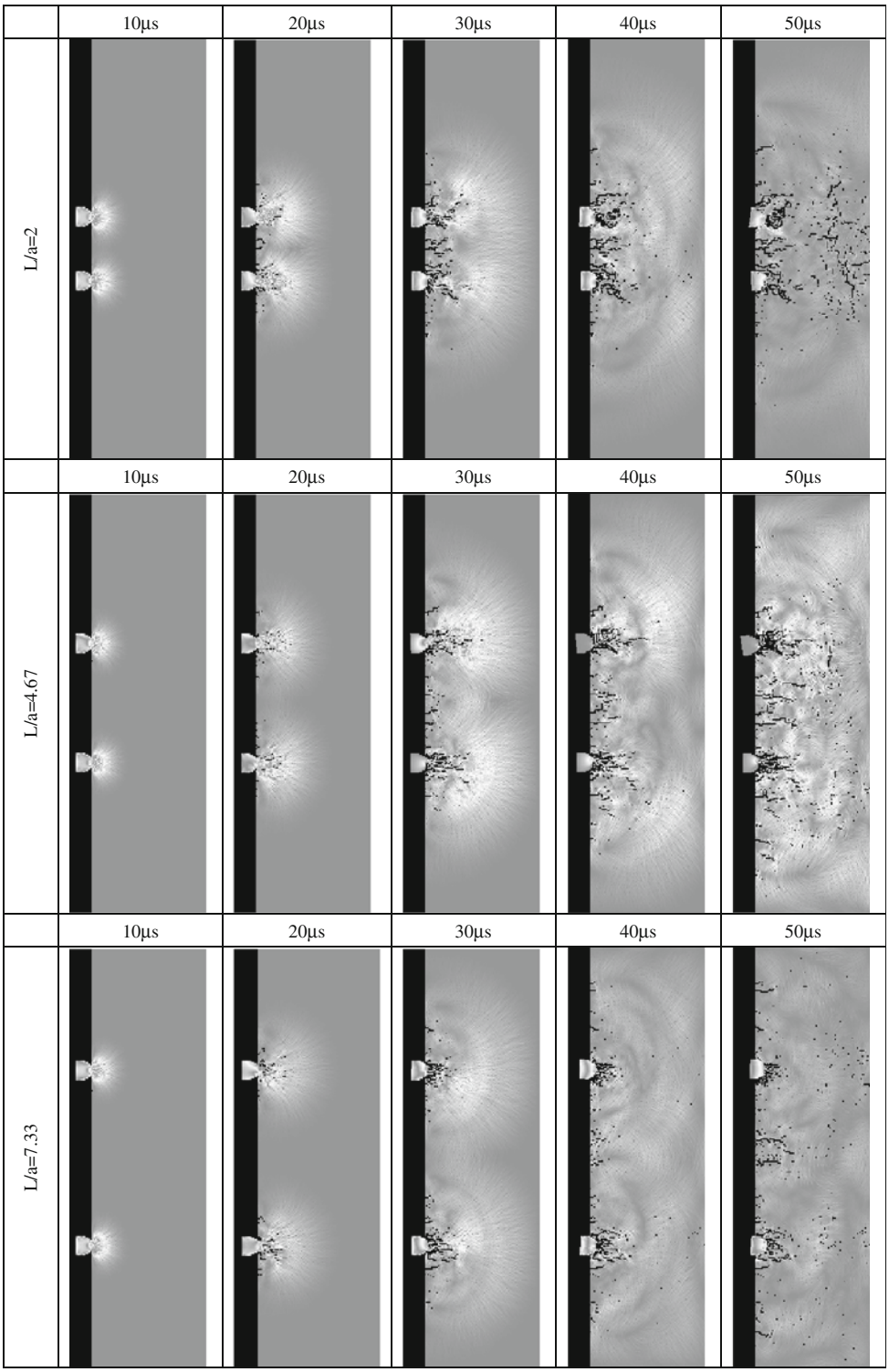

Fig. 17 Numerical simulation of the effect of normalized spacing (L/a) on the failure process of specimens due to two indenters subjected to impact loading ($m = 3$)

usually propagate along a curvilinear path during the failure process. Since heterogeneous rock contains more structural particles, voids and fractures, either pre-existing or induced by stresses, they absorb more energy from the applied compressive stress waves. As a result, the compressive stress wave attenuation is more evident in heterogeneous rock, and the reflected tensile stresses waves are also weak, resulting in smaller new fractures.

(4) With a small normalized spacing, the interaction of the stress fields induced by the two compressive stress waves from double indenters is not complete. Indeed,

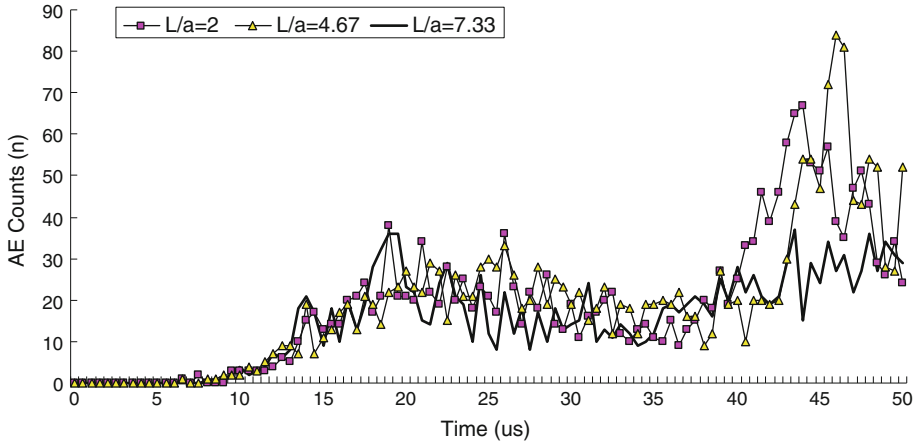

Fig. 18 Numerical simulation of AE counts versus time due to impact loading with maximum pressures of 90 MPa and *L*/*a* of 2.0, 4.67, and 7.33 ($m = 3$)

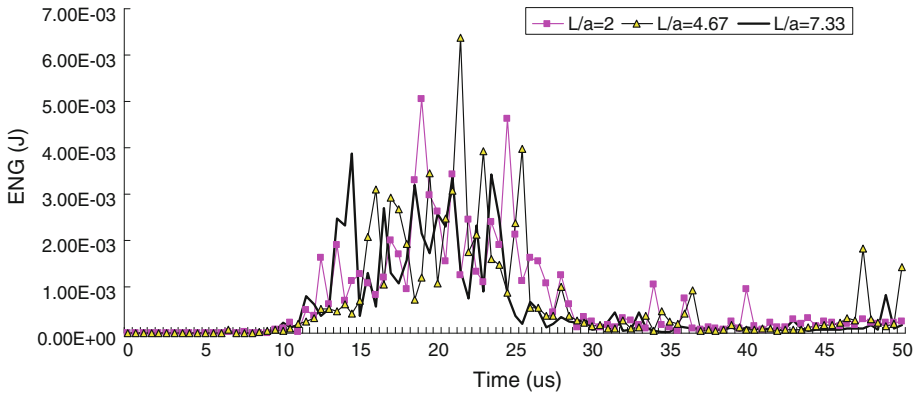

Fig. 19 Numerical simulation of AE energy versus time due to impact loading with maximum pressures of 90 MPa and *L*/*a* of 2.0, 4.67, and 7.33 ($m = 3$)

the propagation of compressive stress waves caused by the double indenters is similar to that caused by a single indenter. With increased spacing, the indenters act independently in the zones adjacent to the indenters and interact with each other in the zone between the indenters. Therefore, the impact loading of the rock surface by multiple indenters with appropriate spacing seems to provide a possibility for forming larger rock chips and consuming a minimum total energy.

Acknowledgments The work described in this article was partially supported by Australian Research Council grant DP0881238, to which the authors are very grateful.

References

Alehossein H, Detournay E, Huang H (2000) An analytical model for the indentation of rocks by blunt tools. Rock Mech Rock Eng 33(4):267–284

Chiang L (2004) Dynamic force–penetration curves in rock by matching theoretical to experimental wave response. J Exp Mech 2:167–175

Cook NGW, Hood M, Tsai F (1984) Observations of crack growth in hard rock loaded by an indenter. Int J Rock Mech Min Sci Geomech Abstr 21(2):97–107

Detournay E, Richard T, Shepherd M (2008) Drilling response of drag bits: theory and experiment. Int J Rock Mech Min Sci 45:1347–1360

Grange S, Forquin P, Mencacci S, Hild F (2008) On the dynamic fragmentation of two limestones using edge-on impact tests. Int J Impact Eng 35:977–991

Han G, Bruno M, Grant T (2005) Dynamically modeling rock failure in percussion drilling. In: Proceedings of the 40th rock mechanics symposium, Anchorage, Alaska, paper ARMA/USRMS 05-819

Hood M, Alehossein H (2000) A development in rock cutting technology. Int J Rock Mech Min Sci 37:297–305

Hustrulid WA, Fairhurst C (1972) A theoretical and experimental study of the percussive drilling of rock. Part III: experimental verification of the mathematical theory. Int J Rock Mech Min Sci 9:417–429

Johnson KL (1985) Contact mechanics. Cambridge University Press, Cambridge

Kou SQ (1995) Some basic problems in rock breakage by blasting and by indentation. PhD thesis, Luleå University of Technology, Sweden

Kumano A (1980) An experimental and analytical investigation of the response of rock to impact loading. PhD thesis, University California, Berkeley, CA

Lindqvist PA (1982) Rock fragmentation by indentation and disc cutting—some theoretical and experimental studies. PhD thesis, Luleå University of Technology, Sweden

Lindqvist PA, Suarez LM, Montoto M, Tan XC, Kou SQ (1994) Rock indentation database—testing procedures, results and main conclusions. SKB report: Pr 44-94-023 Sweden

Liu HY (2004) Numerical modeling of the rock fragmentation process by mechanical tools. PhD Thesis: 32D, Lulea University of Technology, Sweden

Liu HY, Kou SQ, Lindqvist PA, Tang CA (2002) Numerical simulation of the rock fragmentation process induced by indenters. Int J Rock Mech Min Sci 39:491–505

Liu HY, Kou SQ, Lindqvist PA (2008) Numerical studies on Bit-Rock fragmentation mechanisms. Int J Geomech 8(1):45–67

Mishnaevsky LL Jr (1995) Physical mechanisms of hard rock fragmentation under mechanical loading: a review. Int J Rock Mech Min Sci 32(8):763–766

Pang SS, Goldsmith W (1990) Investigation of crack formation during loading of brittle rock. Rock Mech Rock Eng 23:53–63

Paul B, Gangal MD (1969) Why compressive loads on drill bits produce tensile splitting in rock, SPE 2392. In: Proceedings 4th Conference on Drilling and Rock Mechanics, University of Texas at Austin, p 109

Tang CA (1997) Numerical simulation of progressive rock failure and associated seismicity. Int J Rock Mech Min Sci 34:249–262

Tang CA, Kaiser PK (1998) Numerical simulation of cumulative damage and seismic energy release during brittle rock failure. Part I: fundamentals. Int J Rock Mech Min Sci 35(2):113–121

Tang CA, Liu H, Lee PKK, Tsui Y, Tham LG (2000) Numerical tests on micro-macro relationship of rock failure under uniaxial compression. Part I: effect of heterogeneity. Int J Rock Mech Min Sci 37:555–569

Tang CA, Tham LG, Wang SH, Liu H, Li WH (2007) A numerical study of the influence of heterogeneity on the strength characterization of rock under uniaxial tension. Mech Mater 39:326–339

Wagner H, Schumann ERH (1971) The stamp-load bearing strength of rock–an experimental and theoretical investigation. Rock Mech 3(4):185–207

Wang JK, Lehnhoff TF (1976) Bit penetration into rock: a finite element study. Int J Rock Mech Min Sci 13:11–16

Wang SY, Lam KC, Au SK, Tang CA (2006) Analytical and numerical study on the pillar rockburst mechanism. Rock Mech Rock Eng 39:445–467

Wang SY, Sloan SW, Huang ML, Tang CA (2010) Numerical study of failure mechanism of serial and parallel rock pillars. Rock Mech Rock Eng. doi:10.1007/s00603-010-0116-3

Zhao J (2000) Application of Mohr-Coulomb and Hoek-Brown strength criteria to the dynamic strength of brittle rock. Int J Rock Mech Min Sci 37:1115–1121

Zhao XL, Roegiers JC, Passaris EKS (1994) Indentation fracture mechanics and rock disc cutting. In: Proceedings of the 1st North American Rock Mechanics Symposium, June 1–3, 1994, Austin, USA, pp 327–334

Zhu WC, Tang CA (2004) Micromechanical model for simulating the fracture process of rock. Rock Mech Rock Eng 37(1):25–56

Zhu WC, Tang CA (2006) Numerical simulation of Brazilian disk rock failure under static and dynamic loading. Int J Rock Mech Min Sci 43:236–252